Acta Cryst. (1978). A34, 909–921

Testing Aspherical Atom Refinements on Small-Molecule Data Sets*

BY NIELS K. HANSEN AND PHILIP COPPENS

Chemistry Department, State University of New York at Buffalo, Buffalo, New York 14214, *USA*

(*Received* 19 *December* 1977; *accepted* 18 *April* 1978)

X-ray data on silicon, tetracyanoethylene, *p*-nitropyridine *N*-oxide and ammonium thiocyanate are refined with a generalized aspherical-atom formalism as introduced by Stewart, but modified to have a spherical valence more similar to the unperturbed HF valence shell. Several types of radial dependences of the multipole functions are tested and criteria are developed for judging the adequacy of the aspherical-atom refinement. The aspherical-atom model leads to a significant decrease in the least-squares error function, a reduction of features in the residual map, and an improvement in thermal parameters when comparison is made with the neutron results or when the rigid-bond postulate proposed by Hirshfeld is applied. Positional parameters are often improved except in the case of terminal atoms for which discrepancies, attributed to correlation between dipole-population and positional parameters, are sometimes observed. Deformation maps based on the aspherical-atom least-squares parameters contain less noise than $X - N$ maps and benefit from inclusion of calculated values of weak structure amplitudes in the summation. In the cases studied, deformation maps including terms beyond the experimental resolution do not yield additional information.

Introduction

The expansion of the charge density in a crystal in terms of a series of nucleus-centered spherical harmonic functions was first applied by DeMarco & Weiss (1965) and significantly complemented by Dawson (1967) and collaborators in their study of bonding in diamond-type structures. In the earliest treatment the radial function of the valence shell is that of the isolated atom, but the Dawson formalism allows a modified Gaussian radial function for all but the leading spherical term, which is assumed to have the same radial dependence as the isolated atom. A more flexible radial function consisting of a set of harmonic-oscillator wave functions was used by Kurki-Suonio (1968) and applied in the analysis of bonding in diamond, silicon, NaCl, AgCl and CaF_2 (Kurki-Suonio, 1971). Least-squares adjustment of the parameters in the Dawson model was carried out by McConnell & Sanger (1970), while Stewart (1969, 1973*a*) first introduced density basis functions which apply to the atoms at rest rather than the thermally-smeared atoms. In the general case of point symmetry 1, Stewart's functions include a full set of spherical harmonics, truncated at a level chosen by practical considerations such as adequacy in describing the aspherical deformations and available computing facilities.

A related model using angular functions of $\cos^n$ type, which are linear combinations of spherical harmonics, was developed by Hirshfeld (1971) and Harel & Hirshfeld (1975), and applied to a number of organic molecules.

Such models have the obvious merit of providing an analytical description of the charge density and may be used in the calculation of physical properties based on the charge-density distribution (Stewart, 1972). As their use should increase as more accurate data sets become available a critical analysis of the results has been undertaken.

For this analysis we have chosen a number of X-ray and neutron data sets specifically collected for charge-density studies. A program was developed which includes the refinement of all structural, extinction and electron density parameters, the latter up to and including the hexadecapole ($l = 4$) terms. Based on early experience, the spherical component of the valence shell was not described by a single Slater-type exponential expression, but by a function more closely related to the density in the unperturbed, free atom.

The electron density model

The density model consists of a superposition of harmonically vibrating aspherical atomic density distributions:

$$\rho(\mathbf{r}) = \sum_{k}^{\text{atoms}} \rho_k(\mathbf{r} - \mathbf{r}_k - \mathbf{u}) * t_k(\mathbf{u}), \qquad (1)$$

where $t_k(\mathbf{u})$ is a Gaussian thermal-displacement distribution and * indicates a convolution. Each atomic density is described as a series expansion in real spherical harmonic functions through fourth-order (y_{lm}).

$$\rho_{\text{atomic}}(\mathbf{r}) = P_c \rho_{\text{core}} + P_v \kappa'^3 \rho_{\text{valence}}(\kappa' r) + \sum_{l=0}^{4} \kappa''^3 R_l(\kappa'' r) \sum_{m=-l}^{l} P_{lm} y_{lm}(\mathbf{r}/r).$$

* *Electron Population Analysis of Accurate Diffraction Data.* VI. Part V: Cooper, Larsen, Coppens & Giese (1973). *Am. Mineral.* **58**, 21–31.

Table 1. *Real spherical-harmonic functions*

x,y,z are direction cosines.

Order	Symbol	Angular function	Normalization: Density function	Normalization: Wave function
0	00	1	$1/4\pi$	$(1/4\pi)^{1/2}$
1	11+	x	$1/\pi$	$(3/4\pi)^{1/2}$
	11−	y		
	10	z		
2	20	$2z^2-(x^2+y^2)$	$\frac{3\sqrt{3}}{8\pi}$	$\left(\frac{5}{16\pi}\right)^{1/2}$
	21+	zx	$3/4$	$\left(\frac{15}{4\pi}\right)^{1/2}$
	21−	zy		
	22+	xy		
	22−	$(x^2-y^2)/2$		
3	30	$2z^3-3z(x^2+y^2)$	$\frac{10}{13\pi}$	$\left(\frac{7}{16\pi}\right)^{1/2}$
	31+	$x[4z^2-(x^2+y^2)]$	$(\mathrm{ar}^*+14/5-\pi/4)^{-1}$	$\left(\frac{21}{32\pi}\right)^{1/2}$
	31−	$y[4z^2-(x^2+y^2)]$		
	32+	$z(x^2-y^2)$	1	$\left(\frac{105}{16\pi}\right)^{1/2}$
	32−	$2xyz$		
	33+	x^3-3xy^2	$4/3\pi$	$\left(\frac{35}{32\pi}\right)^{1/2}$
	33−	y^3-3yx^2		
4	40	$8z^4-24z^2(x^2+y^2)+3(x^2+y^2)^2$	†	$\left(\frac{9}{256\pi}\right)^{1/2}$
	41+	$x[4z^3-3z(x^2+y^2)]$	$\frac{735}{512\sqrt{7}-196}$	$\left(\frac{45}{32\pi}\right)^{1/2}$
	41−	$y[4z^3-3z(x^2+y^2)]$		
	42+	$(x^2-y^2)[6z^2-(x^2+y^2)]$	$\frac{105\sqrt{7}}{4(136+28\sqrt{7})}$	$\left(\frac{45}{64\pi}\right)^{1/2}$
	42−	$2xy\quad[6z^2-(x^2+y^2)]$		
	43+	$z(x^3-3xy^2)$	$5/4$	$\left(\frac{315}{32\pi}\right)^{1/2}$
	43−	$z(y^3-3yx^2)$		
	44+	$x^4-6x^2y^2+y^4$	$15/32$	$\left(\frac{315}{256\pi}\right)^{1/2}$
	44−	$4x^3y-4xy^3$		

* ar = arctan (2). † $N_{\mathrm{ang}}^{-1}=(14A_-^5-14A_+^5-20A_-^3+20A_+^3+6A_--6A_+)\,2\pi$ where: $A_\pm=\left(\frac{30\pm\sqrt{480}}{70}\right)^{1/2}$.

Here P_c, P_v and P_{lm} are population coefficients. The total number of electrons associated with one atom is equal to $P_c + P_v + P_{00}$, since the higher terms with $l \neq 0$ integrate to zero when integration is performed over all space. The functions ρ_{core} and ρ_{valence} are chosen as the Hartree–Fock (HF) densities of the free atoms normalized to one electron, but the valence function is allowed to expand and contract by adjustment of the variable radial parameter κ' (Coppens, Guru Row, Leung, Stevens, Becker & Yang, 1978; Coppens & Guru Row, 1978).* The radial functions $R_l(r)$ of the other terms are

$$R_l(r)=\frac{\zeta_l^{n_l+3}}{(n_l+2)!}\,r^{n_l}\exp(-\zeta_l r) \qquad (3)$$

where in principle n_l can take any positive integer value. Starting values of the orbital exponent ζ are modified by a variable parameter κ'', such that $\zeta'=\kappa''\zeta$.

The spherical harmonic functions y_{lm} and the normalization factors based on $\int|y_{lm}|d\tau=2$ (except for $l=0$ in which case $\int|y_{lm}|d\tau=1$ is used) are listed in Table 1. This normalization implies that with $P_{lm}=1$ one electron has been moved from the negative to the positive lobes of the deformation functions with $P\geq 1$.

The structure factor expression corresponding to (2) and (3) becomes:

$$F(\mathbf{h})=\sum_k^{\text{atoms}}\sum_p^{\text{symmetry}}\Big[P_c f_{\mathrm{core}}(h)+P_v f_{\mathrm{valence}}(h/\kappa'')+\sum_{l=0}^{4}\Phi_{kl}(h/\kappa'')\sum_{m=-l}^{l}P_{klm}y_{lm}^k(\mathbf{h}_p/h)\Big]\times\exp 2\pi i\,\mathbf{h}.\mathbf{r}_{kp}\,T_k(\mathbf{h}), \qquad (4)$$

* It may be noted that ρ_{core} and ρ_{valence} are constructed from the canonical Hartree–Fock atomic orbitals.

where f_{core} and $f_{valence}$ are the Fourier transforms of ρ_{core} and $\rho_{valence}$ respectively and Φ_{kl} is the Fourier–Bessel transform of R_{kl}, defined as:

$$\Phi_{kl}(h) = 4\pi i^l \int_0^\infty R_{kl}(r) j_l(2\pi hr) r^2 \, dr. \quad (5)$$

The temperature factor T_k is the Fourier transform of t_k, and $\mathbf{h}_p$ and $\mathbf{r}_{lp}$ are symmetry-transformed scattering and position vectors. We note that the model reverts to the free-atom model when $\kappa' = 1$ and the P_{klm}'s are zero. It is in this respect similar to Hirshfeld's deformation model (Harel & Hirshfeld, 1975), but different from the single Slater-type models used by a series of authors (Cromer, Larson & Stewart, 1976; Price & Maslen, 1978; Chen, Trucano & Stewart, 1977).

Expression (4) has been used in a least-squares program *MOLLY* which is an extension of the general structure-refinement program *LINEX*74. The program allows refinement of positional, harmonic-anisotropic-vibration and extinction parameters (according to Becker & Coppens, 1975) as well as the population coefficients P_v, P_{klm} and the radial parameters κ' and κ'' for each atom. Atoms can be constrained to share a set of radial expansion functions. The number of population coefficients can further be reduced by applying chemical symmetry as discussed by Hirshfeld (1971) and Stewart (1973*a*). In the present version of the program the total charge is constrained so that the crystal remains neutral during the refinement.

Criteria for judging aspherical atom refinements

Though an aspherical-atom (multipole) refinement based on expression (1) may lead to a lowering of the agreement indices, the improvement is not necessarily significant because of the large number of parameters involved, and results are not necessarily physically meaningful as they may be affected by parameter correlation or systematic errors in the measurements. The following tests of the multipole refinements have therefore been applied.

(*a*) *Significance of improvement of the fit between calculated and observed structure factors*

For an adequate model the goodness of fit g, defined as

$$g = (\sum w_i \Delta_i^2 / v)^{1/2}, \quad (6)$$

should tend towards 1 as refinement proceeds.

For a refinement on F, Δ equals $|F_{obs}| - |kF_{calc}|$, w_i represents the weight assigned to each of the reflections from an estimate of experimental accuracy and v is the number of degrees of freedom (*i.e.* the number of independent observations n, minus the number of independently varied parameters p).

In comparison of different models we shall use the error function

$$\varepsilon = vg^2 = \sum w_i \Delta_i^2 \quad (7)$$

which follows a χ^2 distribution with v degrees of freedom for a fully refined model. As shown by Hamilton (1964, 5–4) the error function can be tested by a modification of the R-factor test:

$$\frac{\varepsilon' - \varepsilon}{\varepsilon} - \frac{d}{n-p} F_{d,n-p}$$

or

$$\varepsilon'/\varepsilon = 1 + \frac{d}{n-p} F_{d,n-p}, \quad (8)$$

where d is the dimensionality of the hypothesis, and the tabulated F distribution is the ratio of two χ^2 distributions.

(*b*) *Residual density maps*

A residual density map, from a Fourier summation based on $(1/kF_{obs}) - |F_{calc}|$ as is commonly used in structure analysis will show to what extent the multipole expansion has been successful in describing the features of the density distribution. It does not contain information, however, on the significance of residual features. For this purpose the residual density distribution may be compared with a map representing the position dependence of the estimated standard deviation in ρ_{obs} as described by Rees (1976, 1977) and calculated in several previous studies (see, for example, Stevens & Coppens, 1976; Coppens, Yang, Blessing, Cooper & Larsen, 1977).

The error distribution in the observed total density in the plane of the tetracyanoethylene (TCNE) molecule, calculated with a program written by E. D. Stevens, is shown in Fig. 1. As found in earlier studies the error density is relatively constant throughout the unit cell, except near symmetry elements.

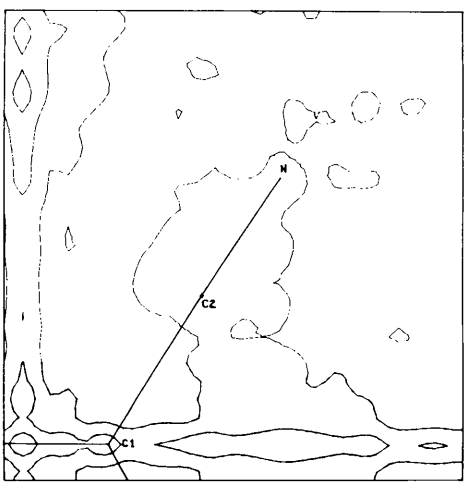

Fig. 1. Distribution of $\sigma(\Delta\rho)$ in the plane of the tetracyanoethylene molecule. Contours at 0·050, 0·0625 and 0·075 e Å^{-3}.

(c) *Parameter bias*

A successful refinement should give parameters with minimal bias due to atomic asphericity. The rationale for this requirement is twofold. First, deformation maps (*i.e.* total minus 'sum of spherical atom' densities) are quite sensitive to errors in positional and thermal parameters, and second, physical properties to be calculated from the refinement results, such as dipole and quadrupole moments, depend on the nuclear positions as well as on the charge distribution.

As a test, parameters from the aspherical-atom refinements are to be compared with neutron diffraction results, while for thermal parameters conformity to the 'rigid-bond postulate' proposed by Hirshfeld (1976) will be examined.

(d) *Comparison of $X - N$ and multipole deformation maps*

A dynamic multipole deformation map, with Fourier components truncated at the experiment resolution may be defined as

$$\Delta\rho_{\text{multipole deformation}}(\mathbf{r}) = \frac{1}{V} \times \sum [\mathbf{F(h)}_{\text{multipole def}} - \mathbf{F(h)}_{\text{spherical atom}}] \times \exp[-2\pi i(\mathbf{h}.\mathbf{r})], \quad (9)$$

where $F_{\text{multipole, deformation}}$ is as defined in (4) and includes the deformation of the spherical valence shell component.

As the $X - N$ and multipole deformation maps represent the same information a comparison of the two functions is a further test of the calculational methods involved.

Both functions are affected by errors in the extinction correction and the scale factor, though in a somewhat different way. Whereas the $X - N$ maps are directly dependent on these factors, they only enter the multipole deformation maps through correlation with other parameters. The promolecule densities (*i.e.* the density corresponding to a superposition of spherical atoms with experimental thermal motion) are also somewhat different in the two cases because the parameters from the neutron and aspherical atom refinements are used respectively. The differences can be summarized as follows:

$$\rho_{\text{def, } X-N} - \rho_{\text{def, multipole}} = \Delta\rho_{\text{scale, extinction}} + \Delta\rho_{\text{promolecule}} + \rho_{\text{residual}}, \quad (10)$$

where the last term is the residual density after completion of the multipole refinement. The first two terms on the right-hand side contribute mostly in the regions near the nucleii, while the residual density may be significant everywhere in the unit cell.

(e) *Derived properties*

One of the justifications for performing the multipole refinement is the experimental determination of derived physical properties (Stewart, 1972). Properties such as net molecular charges, dipole and quadrupole moments may also be obtained by direct-space integration of the experimental charge distribution. A comparison of dipole moments for a number of molecules will be described in a following publication (Guru Row, Hansen and Coppens, to be published).

Table 2. *Survey of data sets and agreement factors*

	Silicon	TCNE	PNPNO	NH_4SCN
Space group	*Fd3m*	*Im3*	*Pnma*	$P2_1/c$
a (Å)	5·430356	9·736 (6)	12·498 (6)	4·138 (2)
b (Å)	5·430356	9·736 (6)	5·814 (2)	7·074 (3)
c (Å)	5·430356	9·736 (6)	7·824 (2)	13·090 (5)
β (°)	–	–	–	97·19 (3)
V (Å^3)	160·135	922·9	568·5 (6)	380·2 (2)
Z	8	6	4	4
Temperature (K)	Room	Room	30	81
λ_X (Å)	0·70930	0·71069	0·71069	0·71069
$(\sin\theta/\lambda)_{\text{max, X-ray}}$ (Å^{-1})	1·04	0·94	1·00†	0·95*
λ_N (Å)	–	1·014	1·445	1·0164
$(\sin\theta/\lambda)_{\text{max, }N}$ (Å^{-1})	–	0·68	0·55	0·70
Number of observations				
X-ray	21	706	2201	3679
Neutron	–	503	451	2716
R factors				
Refinement on	*F*	*F*	F^2	*F*
Conventional/multipole				
R (%)	1·0/0·3	5·9/3·0	5·3/2·9	2·0/1·1
wR (%)	1·6/0·05	4·8/1·8	7·6/4·0	3·2/1·3
Goodness of fit	55·5/1·8	4·5/1·8	1·92/1·10	1·40/1·29

* Not a complete set of reflections measured for $\sin\theta/\lambda > 0{\cdot}75$ Å^{-1}.
† In this data set about 100 reflections are missing in the range $0{\cdot}50 < \sin\theta/\lambda < 0{\cdot}65$ Å^{-1}.

Details on the data sets and least-squares requirements

Data sets on silicon, tetracyanoethylene, *p*-nitropyridine *N*-oxide and ammonium thiocyanate were used in the analysis. Details are summarized in Table 2 and are further discussed below. Some initial refinements showed that the variable valence shell (the 'first' monopole) was sufficiently flexible and that the second 'Slater-type' monopole [$l = 0$ in expression (2)] did not improve convergence. All refinements were therefore limited to one monopole valence function per atom.

(*a*) *Silicon*

The structure factors of silicon are of unusual accuracy. They were measured with the *Pendellösung* fringe method by Aldred & Hart (1973). Four reflections from a similar data set by Hattori, Kuriyama, Katagawa & Kato (1965) were added, as were the intensities of the weak forbidden 222 and 442 reflections as measured by Roberto & Batterman (1970) and Trucano & Batterman (1972) respectively. These 222 and 422 reflections are forbidden according to the spherical-atom model but allowed in more general formalisms such as expression (2). As described by Dawson (1967) and by Stewart (1973*a*), the only multipole deformation functions allowed for the tetrahedral site symmetry of the Si atom are one octapole and one hexadecapole, the latter being a combination of y_{40} and y_{44^+} (Table 1):

$$\rho_{\text{hexadecapole}} = P_{\text{hexa}}\left(y_{40} + \frac{5N_{40}}{N_{44^+}} y_{44^+}\right).$$

For harmonic thermal motion the maximum number of parameters is therefore five ($B, \kappa', \kappa'', P_{\text{octa}}, P_{\text{hexa}}$) and the structure factor expression becomes (for Si at $\frac{1}{8},\frac{1}{8},\frac{1}{8}$):

$$F(\mathbf{h}) = \left[P_c f_{\text{core}}(h) + P_v f_{\text{valence}}\left(\frac{h}{\kappa'}\right) + P_3 \Phi_3\left(\frac{h}{\kappa''}\right)\frac{h_x h_y h_z}{h^3} + P_4 \Phi_4\left(\frac{h}{\kappa''}\right) \times\left(\frac{h_x^4 + h_y^4 + h_z^4}{h^4} - \frac{3}{5}\right)\cos\left(\pi\frac{h_x + h_y + h_z}{4}\right)\right] \times \exp(-B\sin^2\theta/\lambda^2), \quad (11)$$

where h_x, h_y and h_z are the components of $\mathbf{h}$ along the axes of a local atomic coordinate system.

(*b*) *Tetracyanothylene* (*TCNE*)

The electron density analysis of TCNE with both X-ray and neutron diffraction data has been described previously (Little, Pautler & Coppens, 1971; Becker, Coppens & Ross, 1973). As the severe extinction was originally treated with the Zachariasen formalism, both X-ray and neutron refinements have been repeated with the modified formalism of Becker & Coppens (1975). The effect of the improved extinction model is to bring the X-ray and neutron thermal parameters in closer agreement, though the latter are still significantly lower than the X-ray values.

The center of the TCNE molecule occupies a site of *mmm* symmetry, so that only two carbon atoms and one nitrogen are symmetry independent. All symmetry-allowed multipoles up to and including the hexadecapole level were included. The two carbon atoms shared one set of radial functions. With this restriction the total number of parameters is 61.

(*c*) *p-Nitropyridine N-oxide* (*PNPNO*)

The X-ray and the neutron data for PNPNO were measured at 30 K (Wang, Blessing, Ross & Coppens, 1976; Coppens & Lehmann, 1976), but while the X-ray data were collected up to $\sin\theta/\lambda = 1{\cdot}00$ Å^{-1} the neutron data set only extends to $0{\cdot}55$ Å^{-1}. It was found that the noise level in the difference maps based on high-order ($X - X_{\text{HO}}$) and neutron ($X - N$) parameters becomes excessive if reflections above $0{\cdot}75$ Å^{-1} are included. By employing a multipole model, deformation maps without the unwanted noise can be calculated. This is especially desirable in the study of the N—O bond regions, where $X - X_{\text{HO}}$ and $X - N$ maps do not indicate any significant density.

The PNPNO molecule lies in a crystallographic mirror plane. To reduce the number of parameters the multipole coefficients were constrained to obey an additional, local mirror plane perpendicular to the molecule. No constraints were imposed on the positional and thermal parameters, which are more accurately determined than the multipole coefficients, except for those of the hydrogen atoms which were fixed at their neutron diffraction values. For C, N and O atoms all *mm* symmetry-allowed population coefficients up to, and including the hexadecapole level were varied, while for the H atoms only one monopole and a bond-directed dipole were refined. The total number of variables was 154.

(*d*) *Ammonium thiocyanate* (NH_4SCN)

An X-ray and neutron analysis of NH_4SCN has been described by Bats & Coppens (1977). The model for the atoms in the SCN group included all multipoles up to the octapole level plus the hexadecapole functions with cylindrical symmetry around the SCN molecular axis. For the nitrogen atom in the ammonium group only a monopole and the octapole and two hexadecapole functions allowed for tetrahedral symmetry (as described for silicon) were varied, but unlike silicon the relative occupancy of two hexadecapoles was not

Table 3. *Multipole refinements of silicon*

Spherical valence configuration	$3s^23p^2$	$3s^23p^2$	$3s^23p^2$	$3s^13p^3$
ζ_l-coupling model	I identical to III	I	III	III
l	n_l ζ_l	n_l ζ_l	n_l ζ_l	n_l ζ_l
3	4 ζ_3	6 ζ_3	6 ζ_3	6 ζ_3
4	4 ζ_3	8 $\frac{4}{3}\zeta_3$	8 ζ_3	8 ζ_3
$\sum w\Delta^2$	115·5*	51·8	52·0	81·3
$r_{\max,3}$ (Å)	1·01 (2)	0·99 (1)	0·99 (1)	1·00 (1)
U_{iso} (Å^2 × 10^6)	5778 (41)	5742 (27)	5727 (27)	5725 (34)

* Slow convergence.

constrained. The hydrogen atoms were treated as in the case of PNPNO. The two nitrogen atoms were assigned independently variable radial functions. The number of refined parameters was 111.

Choice of radial function coefficients

The multipole model defined by (1) leaves the values of n_l and the relative values of ζ_l for successive multipoles to be selected. The choice of n_l will be mainly based on the origin of the multipole density functions as product of atomic orbitals. A scheme for the orbital exponents was selected on the basis of a series of TCNE refinements.

(*a*) *Choice of n_l for first-row atoms*

Stewart (1977) has shown that if the model with a single exponential radial function is to obey Poisson's electrostatic equations at the atomic nucleus the condition $n_l > l$ must be fulfilled.

If bond density is neglected the multipole density functions can be related to products of atomic orbitals which occur in the quantum-mechanical one-electron density function. Monopolar, dipolar and quadrupolar density functions will result, for example, from *ss*, *sp* and *pp* type orbital products respectively, which suggests the choice of $n_l = 2$ for all three types of functions in the case of first-row atoms.

Similarly, octapoles and hexadecapoles can be thought of as arising from $2p3d$ and $3d3d$ atomic orbital products which would lead to $n_l = 3, 4$ respectively. This argument is of course much weaker as $3d$ orbitals are not occupied for first-row atoms and the higher multipoles in fact solely represent the density in the bonds around an atom. Nevertheless, we have used the following scheme based on the simple orbital-product argument:

	dipole	quadrupole	octapole	hexadecapole
l	1	2	3	4
n_l	2	2	3	4

Table 4. *Multipole refinements of ammonium thiocyanate*

	Model I*	Model II†
$\sum w\Delta^2$	2561	2475
κ'_S	0·973 (5)	0·973 (4)
ζ_S (bohr^{-1})	3·90 (13)	4·40 (12)

Number of reflections included in refinement 1597
Number of parameters refined 111

$$\frac{\varepsilon_I}{\varepsilon_{II}} = \frac{2561}{2475} = 1{\cdot}035;\ 1 + \frac{1}{1486}F_{1,1486,5\%} = 1{\cdot}003$$

Radial function = $Nr^{n_l}\exp(-\zeta r)$, *i.e.* ζ is equal for all multipoles

* Model I: $l = 1\ 2\ 3\ 4$; $n_l(S) = 4\ 4\ 4\ 4$; $n_l(C,N) = 2\ 2\ 3\ 4$.
† Model II: $l = 1\ 2\ 3\ 4$; $n_l(S) = 4\ 4\ 6\ 8$; $n_l(C,N) = 2\ 2\ 3\ 4$.

(*b*) *Choice of n_l for second-row atoms*

For second-row atoms the orbital-product argument leads to $n_l = 4$ for all deformation functions. This means that all radial functions would be identical if all ζ values were equal, whereas in the first-row atom scheme described above the higher poles are more diffuse.

As silicon refinements with only an octapolar deformation function gave a best fit for $n_3 = 6$, a set of n_l values increasing with l: $n_1 = 4$, $n_2 = 4$, $n_3 = 6$, $n_4 = 8$ was compared with the $n_1 = n_2 = n_3 = n_4$ model. The results for silicon and NH_4SCN, summarized in Tables 3 and 4, indicate improved agreement with the more diffuse higher multipoles. Though this search is obviously not exhaustive, its conclusions were confirmed by examination of the residual density maps.

(*c*) *Coupling of ζ_l values of successive multipoles*

In the refinement of TCNE three models for 'ζ coupling' were examined. In the first the ζ's of successive poles were adjusted so that all functions peak at the same distance from their center using the

equality $r_{max} = n_l/\zeta$. In the third model, on the other hand, all orbital exponents were equal for each atom, so that with the n_l values selected above, the higher multipoles peak further away from the atoms on which the multipoles are centered (Fig. 2).

The second model is intermediate with ζ value ratio's which are the average of those of the other two models. The peak positions and ζ values of the three models are illustrated in Fig. 3.

Results of the TCNE refinement (with structural parameters fixed at the neutron diffraction positions) are summarized in Table 5. The best fit of the data is obtained with model III, in which the orbital exponents are the same for all l, and the higher multipoles more diffuse than the dipolar and quadrupolar terms. The improvement is highly significant according to the F test on the error function although it must be emphasized that the tested hypothesis is highly non-linear. For silicon models I and III were tested and were found to fit about equally. A ground state $3s^23p^2$ starting function for the monopole gave better agreement than a prepared state $3s3p^3$ function (Table 3).

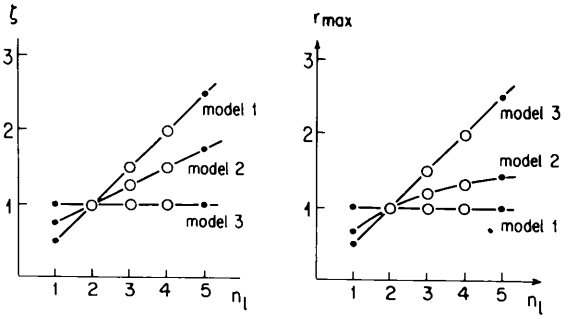

Fig. 3. Relative values of ζ, and position of the radial maxima for the three models described in the text.

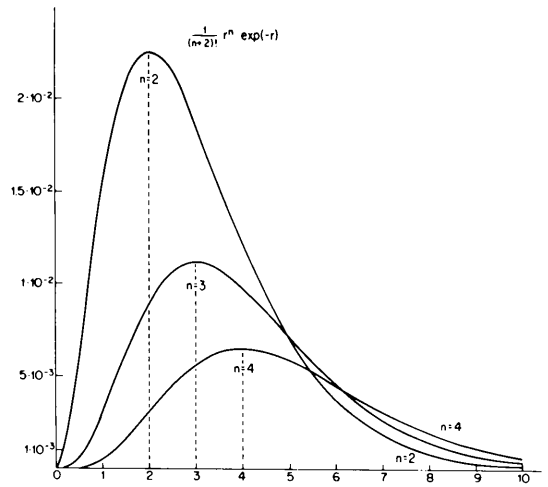

Fig. 2. The radial dependence of the exponential-type function for different values of n. Horizontal axis in units of r.

Table 5. *Multipole refinements of tetracyanoethylene*

Positional and thermal parameters are fixed at neutron values.

	I	II	III
	$\zeta_l = \zeta_0 n_l/2$ r_{max} independent of l	$\zeta_l = \zeta_0 \frac{(1 + n_l/2)}{2}$	$\zeta_l = \zeta_0$ r_{max} proportional to n_l
$\sum w\Delta^2$	1436	1306	1286
κ'_C	1·071 (12)	1·052 (12)	1·062 (11)
κ'_N	1·033 (9)	1·025 (9)	1·021 (8)
ζ_0(carbon)	2·27 (9)	2·25 (7)	2·49 (9)
ζ_0(nitrogen)	4·06 (8)	4·19 (27)	5·14 (37)
Number of reflections included		355	
Number of parameters refined		45	

$$\frac{\varepsilon_I}{\varepsilon_{III}} = 1{\cdot}117;\ 1 + \frac{1}{310} F_{1,310,5\%} = 1{\cdot}012$$

$n_l = 2,2,3,4$ for $l = 1,2,3,4$

Table 6. *Radial parameters of valence shell deformation functions (ζ equal for all l)*

l	1	2	3	4
n_l (1st row atoms)	2	2	3	4
n_l (2nd row atoms)	4	4	6	8

ζ (bohr^{-1})	TCNE	PNPNO	NH_4SCN	Si
C	2·49 (9)	3·15 (10)	2·80 (14)	–
N	5·14 (37)	3·43 (18)	3·60 (21); 3·27 (8)	–
O	–	4·40 (32)	–	–
Si	–	–	–	3·20 (03)
S	–	–	4·40 (13)	–
H monopole		2·48 (8)	2·95 (10)	–
H dipole		4·7 (9)	5·5 (9)	
κ'				
C	1·062 (11)	1·001 (7)	0·992 (8)	–
N	1·021 (8)	1·001 (9)	0·990 (5); 0·943 (6)*	–
O	–	1·002 (4)	–	–
Si	–	–	–	0·956 (9)
S	–	–	0·973 (4)	–

* First value for the cyanide nitrogen, second for ammonium.

We note that formally model III is also in agreement with the orbital-product argument: if the octapolar and hexadecapolar functions would arise from *d* orbitals they would naturally be more diffuse. A physically more acceptable argument is that the higher functions effectively account for density in the covalent bonds which are relatively distant from the nuclear centers. Though our refinements suggest a preference for the choice of more diffuse functions for higher multipoles, the conclusions are without further testing only applicable to first-row atoms. The behavior of transition metals in which *d* orbitals are populated cannot be inferred from these tests.

(*d*) *General comments on* ζ *values*

Radial-parameter values from the refinements are listed in Table 6. Though the expansion–contraction parameter κ' of the first monopole is close to one, a large variation is found in κ'' (and therefore $\kappa''\zeta$) for the same atom in different environments. An analysis of the improvement of fit on variation of κ'' indicates very strongly that such a variation is essential.

Bentley & Stewart (1976) determined ζ values from a multipole analysis of theoretical diatomic molecule densities using restricted radial functions of the type $r^n \exp(-\zeta r)$ common to both the spherical valence shell and the higher deformation functions. When the valence shell and the deformation functions are linked in this way very little variation between ζ values for different molecules is found. However, when higher poles are added successively to the model, as in the experimental analysis of diamond (Stewart, 1973*b*), ζ values decrease, in agreement with our experience that the higher poles should be more diffuse, and preferably not be coupled to the leading term describing the spherical valence shell.

Application of the refinement criteria: the adequacy of the aspherical atom treatment

Goodness of fit and residual densities

In all cases the aspherical-atom formalism leads to a highly significant decrease in the error function ε in comparison with the spherical-atom refinement. There is a corresponding improvement in the residual maps, which, however, fail to give indication of the positional-parameter error of the nitrogen atom in TCNE. As discussed below this error is large and attributed to high correlation between the positional parameters and dipole population coefficients. The residual map gives information on the goodness of the fit and not on the physical significance of the least-squares parameters! Nevertheless, we have found the maps to be useful in judging the completeness of the multipole expansion. In the case of sulfamic acid (NH_3SO_3) they clearly showed residual density on the N—S bond axis when for practical considerations the nitrogen expansion was truncated at the octapole level (Guru Row, Hansen and Coppens, to be published).

Positional parameters

Even though in TCNE the C≡N bond lengths from the neutron and multipole refinements are almost equal [1·145 (1) and 1·146 (4) Å respectively], the agreement between the nitrogen coordinates is poor, as illustrated in Fig. 4. Relative to the neutron result the

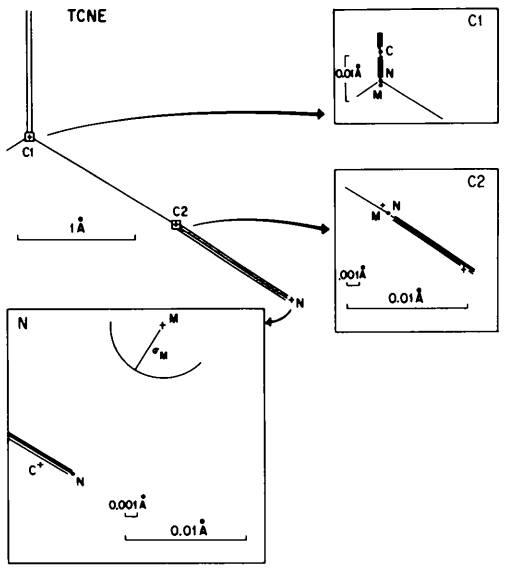

Fig. 4. Positions of the atoms in tetracyanoethylene as obtained from a spherical atom refinement of X-ray data (*C*), a multipole refinement of X-ray data (*M*) and a refinement of neutron data (*N*). Note that the scale in the boxes differs from the overall scale of the figure.

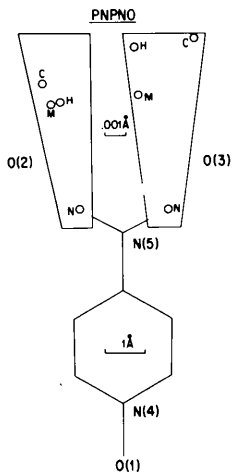

Fig. 5. Positions of the atoms in *p*-nitropyridine *N*-oxide. Symbols as in Fig. 4. *H* indicates results of high-order refinement of X-ray data with $\sin\theta/\lambda > 0{\cdot}75$ Å^{-1}.

nitrogen position from the aspherical atom refinement is displaced by 0·014 Å in a direction perpendicular to the triple bond.

For PNPNO smaller, but similar discrepancies (of 0·005 and 0·006 Å) are observed for the terminal oxygen atoms in the nitro group (Fig. 5). These deviations must be considered significant as the standard deviations of the differences are 0·002 Å. Unlike TCNE, the discrepancies in PNPNO are also found in spherical-atom X-ray refinements. Assuming that the neutron parameters are correct within their statistical error range, the explanation based on comparison of $X - N$ and multipole deformation densities (Fig. 8) is that the multipole model (and of course the conventional spherical-atom model) has not been able to describe the asymmetry of the lone-pair features around the oxygen atoms. As a consequence, these atoms are displaced toward the higher of the two lone-pair peaks.

Mean square discrepancies between sets of PNPNO positional parameters (excluding those of the hydrogen atoms) are summarized in Table 7. The multipole neutron differences are not significant when the oxygen atoms of the nitro group are excluded from the comparison, the allowed deviation in a 95% confidence interval of a χ^2 distribution (with a number of degrees of freedom equal to the number of parameters) being $2{\cdot}31 \times 10^{-3}$ Å. We note that for this set of atoms the multipole parameters appear superior to the spherical-atom and high-order values, as was the case for the carbon atoms in TCNE.

Differences for NH_4SCN are small (Fig. 6), though the multipole geometry again agrees better with the neutron geometry than the results of conventional and high-order refinements.

The bias in the multipole positional parameters seems thus limited to some of the terminal atoms. The difficulty may arise from possibly large correlations between positional and dipole population parameters (Stewart, 1976). To analyze this correlation we have transformed the variance–covariance matrix to refer to the positional parameters in the same local coordinate systems in which the multipole deformation functions are defined. These local orthogonal systems are chosen such that the z axis is along a bond. The transformation results show that cross terms, such as $\mathrm{cov}(y, P_z)$ are small (less than 0·20) while some of the terms referring to the same directions [such as $\mathrm{cov}(z, P_z)$] are appreciable (Table 8). Very high correlations are observed for the nitrogen atom in TCNE. With such large correlations (up to 0·97) the actual parameter values will be very sensitive to even small errors in the structure amplitudes, and the large discrepancy in the nitrogen position can be understood.

Table 7. *Comparisons of geometries of the p-nitropyridine N-oxide molecule from various refinements (values in* $Å^{-3} \times 10^{-3}$)

$$\Delta = \left(\frac{1}{n} \sum_{i=1}^{n} |\mathbf{r}_{1i} - \mathbf{r}_{2i}|^2 \right)^{1/2}$$

	Spherical atom–neutron	High order (>0·75 $Å^{-1}$)–neutron	Multipole–neutron
Without oxygens of nitro group	3·2	2·9	2·4
All atoms	4·6	4·0	3·3

Thermal parameters

The thermal parameters from the different refinements can be compared using two statistical approaches. We may test the value of

$$\Delta_m = n^{-1/2} \sum_{i=1}^{n} \left[\frac{x_{1i} - x_{2i}}{\sigma(x_{1i} - x_{2i})} \right]$$

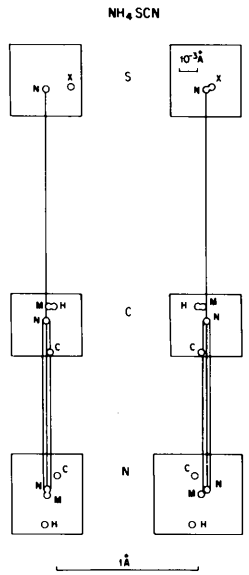

Fig. 6. Positions of the atoms in ammonium thiocyanate in two perpendicular planes through the CNS group. Symbols as in Figs. 4 and 5. High-order refinement of data with $\sin\theta/\lambda > 0{\cdot}65$ $Å^{-1}$. All X-ray positions for sulfur are identical.

Table 8. *Correlation between positional parameters and dipole population coefficients*

x,y refers to directions perpendicular to bonds, z refers to directions parallel to bonds.

		x–P_x	y–P_y	z–P_z
TCNE	C(2)	–	−0·65	−0·52
	N	–	−0·97	−0·95
PNPNO	O(1)	–	–	−0·71
	O(2)	–	−0·70	−0·60
	O(3)	–	−0·71	−0·65
NH_4SCN	S	−0·40	−0·47	−0·35
	C	−0·53	−0·59	−0·33
	N	−0·73	−0·79	−0·63

Table 9. *Comparison of thermal parameters*

	Spherical atoms–neutron		High order–neutron		Multipole–neutron		Δ_m, 95% interval	S, 95% interval
	Δ_m	χ	Δ_m	χ	Δ_m	χ		
TCNE								
All atoms	10·93	4·93			2·18	1·85	−1·96 to 1·96	0·55 to 1·45
Only carbon	7·19	4·08			−0·45	1·49	−1·96 to 1·96	0·45 to 1·55
PNPNO	1·32	1·09	1·51	1·11	−1·38	1·22	−1·96 to 1·96	0·75 to 1·25
NH_4SCN								
SCN only	2·03	2·41	3·99	1·99	2·93	1·49	−1·96 to 1·96	0·55 to 1·45
N–SCN	2·76	2·29	4·79	2·13	2·80	1·85	−1·96 to 1·96	0·61 to 1·39

Table 10. *Rigid-bond test of thermal parameters (u^2 in Å^2 × 10^4 in direction of bond)*

$u^2_{\text{bond}} = \mathbf{e}_b^t\ \mathbf{U}\ \mathbf{e}_b$, $\mathbf{e}_b$ being a covariant unit vector in the direction of the bond.

Refinement				
TCNE	C_1——C_2≡≡≡N			r.m.s. discrepancy
Conventional	279	311	341	31·0
Multipole	235	224	179	32·7
Neutron	230	233	229	4·1
NH_4SCN	S——C≡≡≡N			r.m.s.
Conventional	90	119	115	20·7
High order (>0·60)	91	99	99	5·7
Multipole	91	91	93	1·0
Neutron	91	87	89	3·2
PNPNO	N_4–O_1	N_5–O_2	N_5–O_3	r.m.s.
Conventional	46–28	72–51	66–42	20·5
High order (>0·75 Å^{-1})	43–40	65–59	59–58	3·9
Multipole (Hirschfeld, 1976)	41–38	63–56	58–50	6·4
Multipole (present study)	39–44	58–58	51–52	2·9
Neutron	50–59	75–64	63–39	16·1

$$\text{r.m.s.} = \left[\frac{1}{n}\sum_{i=1}^{n}(u^2_{Ai} - u^2_{Bi})^2\right]^{1/2}$$

against a normal distribution with zero mean and standard deviation one, or the quantity

$$nS^2 = \sum_{i=1}^{n}\left[\frac{x_{1i} - x_{2i}}{\sigma(x_{1i} - x_{2i})}\right]^2$$

against a χ^2 distribution with n degrees of freedom. In both expressions the sets x_{1i} and x_{2i} represent the thermal parameters from two different refinements.

The X-ray and neutron thermal parameters are compared in Table 9. There is no clear trend in Δ_m for the multipole and neutron refinements, Δ_m being negative for TCNE (carbon atoms only) and PNPNO and positive for NH_4SCN. In this last case the deviation from zero is significant, indicating that the multipole (and other X-ray) temperature parameters are generally higher than the neutron values. We note that especially the χ estimator indicates less scatter of the multipole results around the neutron values than is the case for high-order and conventional parameters.

A more physical criterion is provided by the 'rigid-bond postulate' proposed by Hirshfeld (1976). It states that for two atoms covalently bonded to each other their mean square amplitude of atomic vibration in the bond direction should be identical.

If the rigid-bond postulate is valid it should be obeyed by the neutron parameters as well, since these are not biased by the electron density distribution. Data summarized in Table 10 indicate this to be true in all cases within twice the standard deviations.

The vibrational amplitudes from the multipole refinement are in good agreement with the rigid-bond postulate. Except for TCNE there is a striking improvement relative to the full-data spherical-atom results.

Comparison of multipole and $X - N$ deformation maps

Since the deformation functions used are smooth functions the multipole deformation map [defined by expression (9)] may be expected to be free of some of the noise present in $X - N$ maps which are calculated more directly from the experimental data. Such 'noise filtering' is apparent in Figs. 7, 8 and 9 in which the two types of dynamic deformation functions are composed.

Except for TCNE, for which the large parameter shift of the nitrogen atom is evident, the agreement between $X - N$ and multipole maps is good. The largest improvement is obtained in the PNPNO multipole deformation map ($\sin\theta/\lambda < 0{\cdot}65$ Å^{-1}), in which the random features of the $X - N$ map have disappeared. This is attributed to the noise-filtering, and also to the inclusion of many very weak reflections which were omitted from the $X - N$ density because of their relatively large experimental standard deviations.

An additional uncertainty in the $X - N$ maps originates from errors in the phases as calculated from the promolecule density. Examination of the structure factor lists for PNPNO and NH_4SCN shows a few

changes in sign between the promolecule and multipole model structure factors. The corresponding error in the density in these cases is estimated to be less than 0·02 e Å^{-3} anywhere in the unit cell. But the effect on the $X - N$ map is more severe for non-centrosymmetric structures (Coppens, 1974). The dependence of the phases of non-centrosymmetric crystals on details of the multipole model remains to be investigated.

The ability to obtain improved deformation maps must be considered a major consideration in favor of the aspherical atom refinement. But the experience with TCNE shows that such maps should not be accepted without critical examination of the multipole refinement's parameters.

Effect of resolution on the multipole maps of PNPNO

Though the *p*-nitropyridine *N*-oxide X-ray data extend to sin $\theta/\lambda = 1{\cdot}00$ Å^{-1} the map discussed above only contains reflections up to 0·65 Å^{-1}, as inclusion of further high-order reflections in the $X - N$ maps leads to a greatly increased noise level. The multipole deformation maps are not subject to this limitation and two additional maps with cut-off of 1·00 Å^{-1} (Fig. 10*a*) and 1·20 Å^{-1} (Fig. 10*b*) were therefore calculated.

The most impressive difference between Fig. 10*a* (sin $\theta/\lambda < 1{\cdot}00$ Å^{-1}) and Fig. 8(*b*) (sin $\theta/\lambda < 0{\cdot}65$ Å^{-1}) is the sharpening of the N—O bond and oxygen lone-pair peaks upon inclusion of high-order reflections. This is a clear demonstration of the persistence of valence scattering into the high-order region in agreement with

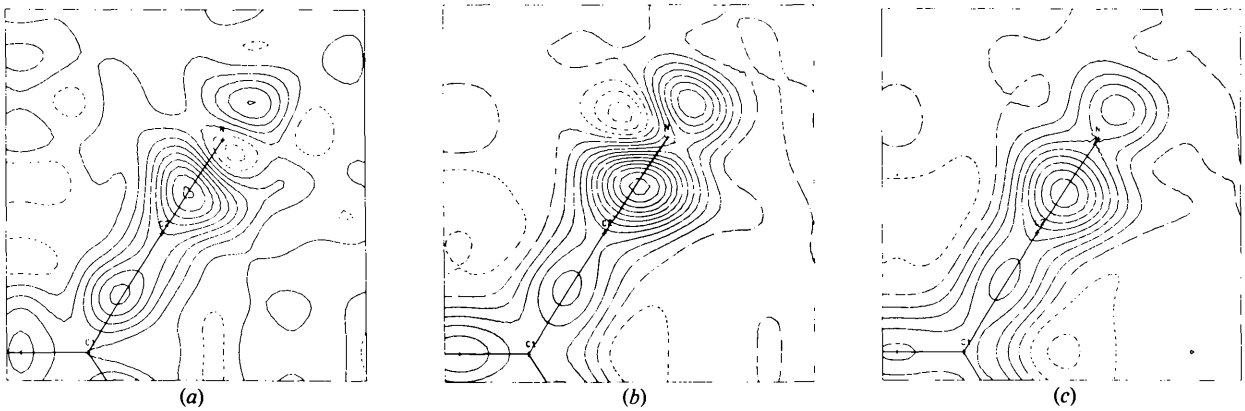

Fig. 7. Deformation density in the plane of tetracyanoethylene based on reflections with sin $\theta/\lambda < 0{\cdot}75$ Å^{-1}. (*a*) $X - N$ deformation density. (*b*) Multipole deformation density. (*c*) As (*b*) but from refinement with positional and thermal parameters fixed at neutron values. Contour interval 0·10 e Å^{-3}. Negative contours broken.

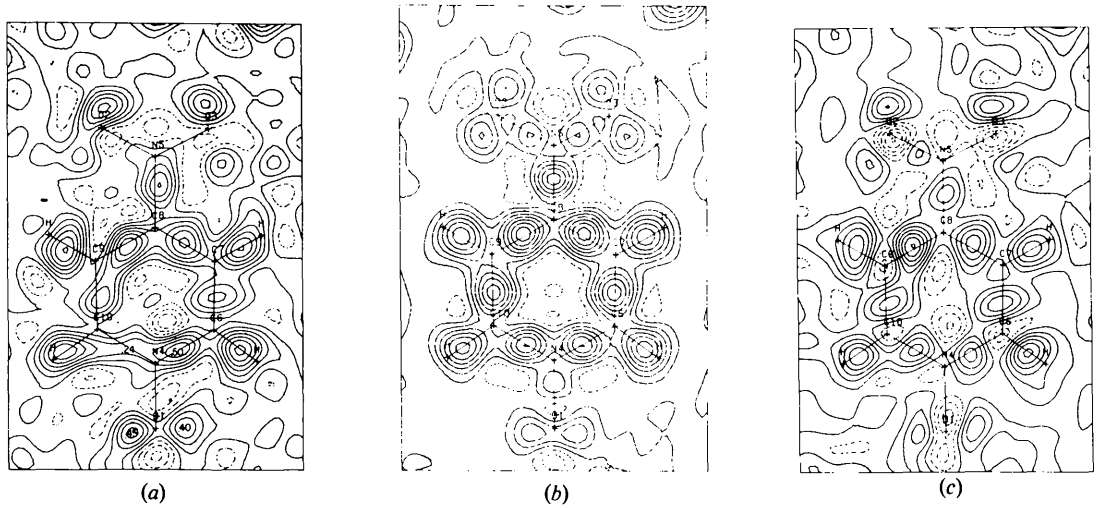

Fig. 8. Deformation density in the plane of the *p*-nitropyridine *N*-oxide molecule based on reflections with sin $\theta/\lambda \leq 0{\cdot}65$ Å^{-1}. (*a*) $X - N$ deformation density (observed reflections only). (*b*) Multipole deformation density (all reflections within sphere). (*c*) As (*b*) but with positional and thermal parameters fixed at neutron values, (observed reflections only). Contours as in Fig. 7.

earlier conclusions (Coppens & Lehmann, 1976), and explains why no N–O bond peaks were found in the $X - N$ map at limited resolution. The peaks in the other bonds become more elongated along the bond direction when resolution is improved, in the case of C–N this is accompanied by a polarization of the bond density, the bond peak in all three C–N bonds moving closer to the more electronegative nitrogen atom.

Very little difference is observed, on the other hand, between the two high-resolution maps, the second of which extends the model density beyond the experimental limit. This suggests that the restricted multipole model including thermal smearing may not describe features that are sharper than what is implied by the experimental resolution. This conclusion is supported by similar experience upon increasing the cut-off in the NH_4SCN model map from 0·75 to 1·10 Å^{-1}.

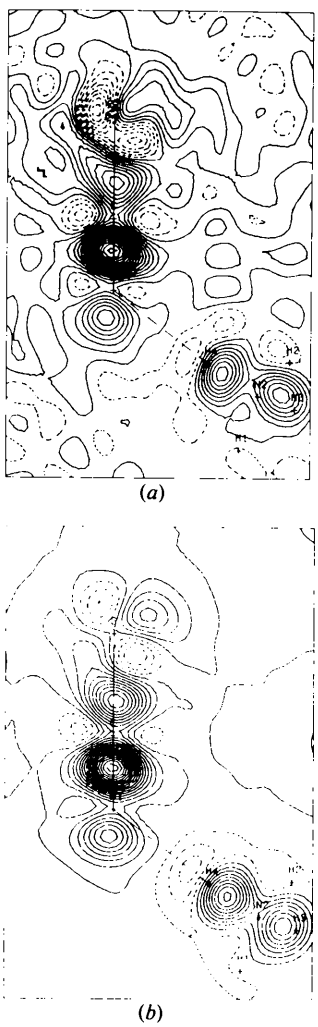

Fig. 9. Deformation density through the SCN ion in ammonium thiocyanate based on reflections with sin $\theta/\lambda \leq 0{\cdot}75$ Å^{-1}. (*a*) $X - N$ deformation density. (*b*) Multipole deformation density. Contour interval 0·05 e Å^{-3}. Negative contours broken.

Refinements with fixed positional and thermal parameters

For TCNE and PNPNO a number of refinements were carried out with the positional and thermal parameters fixed at the neutron values. As may be anticipated the corresponding multipole deformation maps show differences near the atomic positions when comparison is made with the all-parameter refinements.

In PNPNO especially, often sharp features near the atomic positions resulted. Fox, Craven & McMullen (1977) have reported that a good fit to X-ray data on parabanic acid with neutron positions fixed, required addition of a sharp dipole function to the multipole expansion for the oxygen atoms. This appears to be similar to our experience and could reflect random errors in the neutron parameters instead of a true polarization of the oxygen atoms. By fixing the parameters at neutron values experimental uncertainties in the neutron experiment are not properly taken into account. An attractive solution to this problem appears to be the joint refinement of X-ray and neutron data in the multipole approximation. Such refinement with a modification of the program *MOLLY* will be discussed in a future publication (Price, Hansen and Coppens, to be published).

Concluding remarks

The aspherical atom refinement leads to a significantly improved and in general physically meaningful fit to the experimental data. The deformation maps obtained contain less noise and often show more detail due to inclusion of weak reflections than $X - N$ maps. But some caution is necessary because the multipole expansion may be incomplete with respect to detail present in the data set and the refinement sometimes leads to erroneous positional parameters, especially in the case of terminal atoms. Such occurrences may be recognized, however, by examination of residual maps and by comparison of parameters with those from other X-ray and neutron refinements. With these precautions the multipole model may be used to obtain molecular dipole and quadrupole moments. Such applications are presently being explored.

The authors acknowledge stimulating discussions with Drs E. D. Stevens, P. F. Price and T. N. Guru Row. They are also grateful for support of this work by the National Science Foundation (CHE-7613342A01) and the Danish Natural Science Research Council which provided a fellowship to NKH.

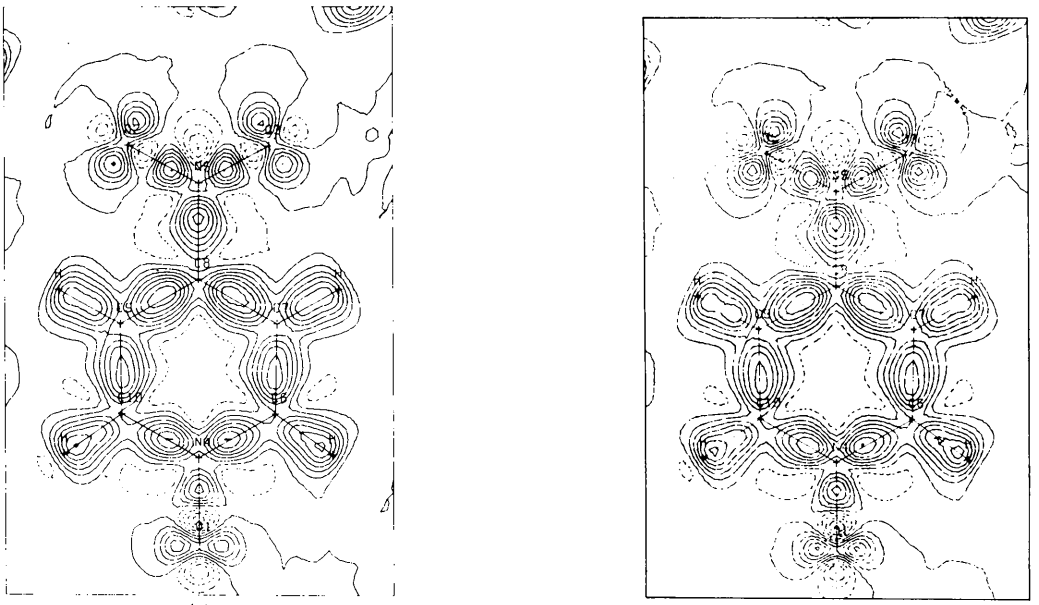

(a) (b)

Fig. 10. Multipole deformation maps in the plane of the *p*-nitropyridine molecule (all reflections within sphere included). (*a*) sin $\theta/\lambda \leq 1{\cdot}00$ Å^{-1}. (*b*) sin $\theta/\lambda \leq 1{\cdot}20$ Å^{-1}. Contours as in Fig. 7.

References

ALDRED, P. J. E. & HART, M. (1973). *Proc. R. Soc. London Ser. A*, **332**, 223–238.

BATS, J. W. & COPPENS, P. (1977). *Acta Cryst.* B**33**, 1542–1548.

BECKER, P. J. & COPPENS, P. (1975). *Acta Cryst.* A**31**, 417–425.

BECKER, P. J., COPPENS, P. & ROSS, F. K. (1973). *J. Am. Chem. Soc.* **95**, 7604–7609.

BENTLEY, J. & STEWART, R. F. (1976). *Acta Cryst.* A**32**, 910–914.

CHEN, R., TRUCANO, P. & STEWART, R. F. (1977). *Acta Cryst.* A**33**, 823–828.

COPPENS, P. (1974). *Acta Cryst.* B**30**, 255–261.

COPPENS, P. & GURU ROW, T. N. (1978). *Trans. NY Acad. Sci. USA*. In the press.

COPPENS, P., GURU ROW, T. N., LEUNG, P., STEVENS, E. D., BECKER, P. J. & YANG, Y. W. (1978). *Acta Cryst.* A. In the press.

COPPENS, P. & LEHMANN, M. S. (1976). *Acta Cryst.* B**32**, 1777–1784.

COPPENS, P., YANG, Y. W., BLESSING, R. H., COOPER, W. F. & LARSEN, F. K. (1977). *J. Am. Chem. Soc.* **99**, 760–766.

CROMER, D. T., LARSEN, A. C. & STEWART, R. F. (1976). *J. Chem. Phys.* **65**, 336–349.

DAWSON, B. (1967). *Proc. R. Soc. London Ser. A*, **298**, 255–263, 264–288.

DEMARCO, J. J. & WEISS, R. J. (1965). *Phys. Rev. Sect. A*, **137**, 1869–1871.

FOX, R. O., CRAVEN, B. M. & MCMULLEN, R. K. (1977). ACA Program Abstr. Ser. 2, Vol. 5, pp. 81–82.

HAMILTON, W. C. (1964). *Statistical Methods in Physical Sciences*. New York: Ronald.

HAREL, M. & HIRSHFELD, F. L. (1975). *Acta Cryst.* B**31**, 162–172.

HATTORI, H., KURIYAMA, H., KATAGAWA, T. & KATO, N. (1965). *J. Phys. Soc. Jpn*, **20**, 988–996.

HIRSHFELD, F. L. (1971). *Acta Cryst.* B**27**, 769–781.

HIRSHFELD, F. L. (1976). *Acta Cryst.* A**32**, 239–244.

KURKI-SUONIO, K. (1968). *Acta Cryst.* A**24**, 379–390.

KURKI-SUONIO, K. (1971). *Analyses of Crystal Atoms on the Basis of X-ray Diffraction*, Ital. Crystallogr. Assoc. Meet. Bari, Italy.

LITTLE, R. G., PAUTLER, D. & COPPENS, P. (1971). *Acta Cryst.* B**27**, 1493–1499.

MCCONNELL, J. F. & SANGER, P. L. (1970). *Acta Cryst.* A**26**, 83–93.

PRICE, P. F. & MALSEN, E. N. (1978). *Acta Cryst.* A**34**, 173–183.

REES, B. (1976). *Acta Cryst.* A**32**, 483–488.

REES, B. (1977). *Isr. J. Chem.* **16**, 180–186.

ROBERTO, J. B., & BATTERMAN, B. W. (1970). *Phys. Rev. B*, **2**, 3220–3226.

STEVENS, E. D. & COPPENS, P. (1976). *Acta Cryst.* A**32**, 915–917.

STEWART, R. F. (1969). *J. Chem. Phys.* **51**, 4569–4577.

STEWART, R. F. (1972). *J. Chem. Phys.* **57**, 1664–1668.

STEWART, R. F. (1973*a*). *J. Chem. Phys.* **58**, 1668–1676.

STEWART, R. F. (1973*b*). *J. Chem. Phys.* **58**, 4430–4438.

STEWART, R. F. (1976). *Acta Cryst.* A**32**, 565–574.

STEWART, R. F. (1977). *Isr. J. Chem.* **16**, 114–131.

TRUCANO, P. & BATTERMAN, B. W. (1972). *Phys. Rev. B*,**6**, 3659–3666.

WANG, Y., BLESSING, R. H., ROSS, F. K. & COPPENS, P. (1976). *Acta Cryst.* B**32**, 572–578.